Stress Path dependence of Ultrasonic and Seismic Velocities in Shale

Rune M Holt, NTNU; Andreas Bauer, SINTEF and NTNU; Audun Bakk, SINTEF; and Dawid Szewczyk, NTNU*

Summary

4D seismic time-shifts are induced by stress changes in the overburden as a result of depletion from or injection into an underlying reservoir. This represents a powerful technique for tracking unrecovered hydrocarbon resources or identifying leakages from CO_2 storage sites. Here we describe how the sensitivity of seismic velocities of overburden shale to reservoir pore pressure changes can be estimated from laboratory experiments. Both ultrasonic and seismic frequency laboratory measurements show stress and stress path dependent velocities. The role of the stress path is seen to be extremely important, which means that geomechanical modeling is required in order to assess *in situ* stress sensitivity. The experiment presented here shows higher stress sensitivity in the seismic frequency range than for ultrasonic waves.

Introduction

Time-lapse (4D) seismic time shifts occur as a result of stress changes in the overburden, caused by pore pressure changes in an underlying reservoir (Hatchell and Bourne, 2005; Barkved and Kristiansen, 2005; Røste *et al*, 2006). The primary response to depletion is a slow-down due to vertical stress reduction associated with stress arching (Kenter *et al*., 2004), whereas a speed-up is expected if the reservoir pore pressure is increased. The amount of slow-down or speed-up depends on the stress sensitivity of the caprock itself, and on the stress path followed by the overburden during reservoir depletion. One may define the changes in terms of vertical and horizontal stress path coefficients, defined as:

$$\gamma_{\mathrm{v}} = \frac{\Delta\sigma_{\mathrm{v}}}{\Delta p_{\mathrm{f(res)}}} \qquad (1)$$

$$\gamma_{\mathrm{h}} = \frac{\Delta\sigma_{\mathrm{h}}}{\Delta p_{\mathrm{f(res)}}}$$

σ_{v} and σ_{h} are the vertical and horizontal stresses, respectively, while $\Delta p_{\mathrm{f(res)}}$ refers to the pore pressure change in the reservoir. The overburden stress path is described further below.

In the following we will show how P-and S-wave velocities measured on shale specimens in the laboratory change with stress and with relevant stress paths. The results will be translated into field situations through simple geomechanical modeling. In most cases, laboratory data are obtained only at ultrasonic frequencies. Here, however, we will also show data obtained from a forced-oscillator low frequency set-up, and from those derive the stress and stress path sensitivities as for the ultrasonic velocities.

Rock physics background

Several approaches have been made in order to model stress dependent velocities in shale (e.g. Sayers, 1999; Prioul et al., 2004). Most models are based on experimental data acquired in hydrostatic tests only, and with no calibration against other stress paths. Sayers (2006) addressed the impact of reservoir stress path on time-lapse seismic, but only considered the response of the reservoir rock itself.

Here, we demonstrate that stress path dependence may be captured simply by assuming that velocities $\mathrm{v_j}$ (where subscript j denotes P-or S-waves in any direction) change linearly with stress:

$$\frac{\Delta \mathrm{v_j}}{\mathrm{v_j}} = A_{\mathrm{j}}\Delta\bar{\sigma} + B_{\mathrm{j}}\Delta(\sigma_z - \sigma_r) - C_{\mathrm{j}}\Delta p_f \,. \qquad (2)$$

$\Delta\bar{\sigma}$ is the change in mean stress. σ_{z} and σ_{r} denote axial and radial stresses in a cylindrical geometry, like that used in triaxial laboratory tests. The pore pressure in the sample is p_{f}. This expression honors the physical mechanisms that control stress sensitivity. The limitation may of course be the assumption of linearity. However, our main target is to apply this to time-lapse seismic interpretation, where the stress and pore pressure changes in the overburden are expected to be small. Further, shales often show close to linear stress dependence over large ranges of stress (Johnston, 1987; Holt *et al*., 2005).

The assumption above implies that the velocity change is also linear in the stress path coefficient $\kappa = \Delta\sigma_{\mathrm{r}}/\Delta\sigma_{\mathrm{z}}$. Eq. (2) can be rewritten as:

$$\frac{\Delta \mathrm{v}_j}{\mathrm{v}_j \Delta\sigma_z} = \frac{1+2\kappa}{3} A_j + (1-\kappa) B_j - C_j \frac{\Delta p_f}{\Delta\sigma_z} \,. \qquad (3)$$

If several different stress paths are probed, and the pore pressure change is measured for each stress path, then the coefficients *A*j, *B*j and *C*j may be estimated from

experiments, and velocity changes may be predicted for any stress path.

In 4D seismic interpretation, the strain sensitivity of velocities may be simplified by the *R*-parameter (Hatchell and Bourne, 2005; Røste *et al*., 2006). For a P-wave travelling in the z-direction, it relates to the strain ε_z in the same direction:

$$R_{Pz} = \frac{\Delta v_{Pz}}{v_{Pz}\Delta\varepsilon_z}. \qquad (4)$$

The stress path sensitivity of *R* can be deduced by rewriting Eq. (4) as

$$R_{Pz} = \left(\frac{\Delta v_{Pz}}{v_{Pz}\Delta\sigma_z}\right)\left(\frac{\Delta\sigma_z}{\Delta\varepsilon_z}\right) \qquad (5)$$

In addition to the contribution from Eq.(3), contained in the first parenthesis, the stress path influences *R* through the stiffness of the material (in the second parenthesis). The representative stiffness is given by Young's modulus for a uniaxial loading path and by the uniaxial compaction modulus for a uniaxial strain path, and furthermore related to the bulk modulus for an isostatic stress path and to the shear modulus for a constant mean stress path.

Geomechanics background

Changes in overburden stresses can be estimated from the nucleus of strain theory of Geertsma (1973), where he described a depleting reservoir in a linearly elastic and homogeneous subsurface. Because of the lack of elastic contrast, this model always gives constant mean stress in the surroundings of the depleting zone, i.e. $\gamma_v+2\gamma_h = 0$. It shows, that stress arching (expressed by $\gamma_v > 0$) increases with increasing ratio between the thickness and the diameter (aspect ratio) of the zone where pore pressure is altered (by depletion or injection)

In order to consider more realistic situations, numerical modeling is needed. Mulders (2003) performed a series of finite element (FEM) simulations, assuming isotropic linear elasticity, varying the elastic contrast between a disk shaped reservoir and its surroundings. The influence of reservoir tilt was also addressed. The results of these simulations were fitted into simple analytical descriptions by Mahi (2003).

Figure 1 shows stress path coefficients in the overburden at the top (center) of a reservoir, based on this approach. The thickness over diameter ratio of the reservoir (aspect ratio) is 0.10, and the reservoir is placed at 3000 m depth. Poisson's ratio was set to 0.30 for the full subsurface, so that elastic contrast represents contrast in either Young's moduli, shear moduli or bulk moduli. The figure demonstrates that stress arching (γ_v) is increasing with increasing elastic contrast and with increasing tilt. γ_h increases slightly with increasing elastic contrast, but decreases with increasing tilt. Notice that for elastic contrast larger than about 2, γ_h changes sign, so that bot vertical and horizontal stress in the overburden will decrease as a result of pore pressure depletion. Skempton's parameters A_S and B_S (Skempton, 1954) may be used to assess the change in pore pressure in the overburden:

$$\Delta p_{f(ovb)} = B_S\left[\Delta\sigma_3 + A_S(\Delta\sigma_1 - \Delta\sigma_3)\right]. \qquad (6)$$

Here σ_1 and σ_3 denote respectively the maximum and minimum principal stress.

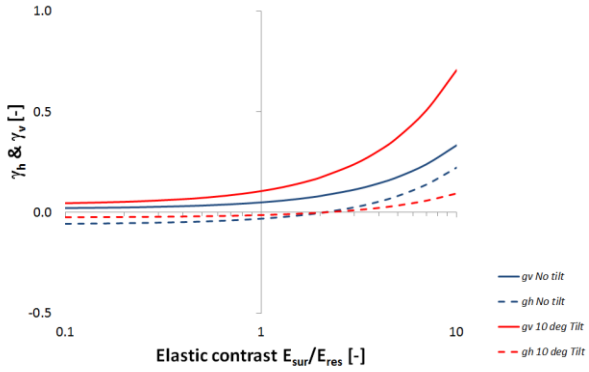

Figure 1: Overburden stress path coefficients γ_v and γ_h as a function of elastic stiffness contrast, derived on the basis of FEM simulations (Mahi, 2003; Mulders, 2003). One case is for a reservoir with a vertical axis, and the other for a reservoir that is tilted by 10°.

Laboratory techniques: Ultrasonic and Seismic frequency measurements

Multidirectional ultrasonic (~ 0.5 MHz) P- and S-wave pulse transmission experiments have been done with cylindrical shale core plugs in a triaxial cell. The data permit determination of all 5 elastic coefficients for the case of transverse isotropy. Measurements are performed along 4 different stress paths: Constant mean stress (CMS), κ = -½; triaxial (3AX), κ = 0; uniaxial strain (K_0), $\kappa = K_0$; and isostatic (ISO), κ = 1. All these sequences were done as undrained loading–unloading cycles, starting from the anticipated *in situ* stress and pore pressure for field cores. Pore pressure response is measured, along with axial and radial strains, plus the confining pressure increase (given by K_0) for the uniaxial strain path.

Stress Path dependence of Ultrasonic and Seismic Velocities in Shale

In addition, quasi-static loading experiments at frequencies 1 – 150 Hz with axial strain amplitudes < 10^{-6} were performed in another triaxial cell. With three (assumed identical) core plugs of different orientations, two Young's moduli and three Poisson's ratios can be determined (e.g. Holt *et al*., 2015). These data are used along with bulk densities to calculate P- and S-wave velocities in the seismic frequency band. Here we will compare not only seismic and ultrasonic velocities, but also seismic and ultrasonic stress and stress path sensitivities.

Experimental data: Ultrasonic measurements

Figure 2 shows measured stress sensitivity and measured *R*-factor for four different stress paths, obtained with a field shale core, with the z-axis normal to the bedding plane. Within experimental uncertainty, the linear trend in stress path is observed for the stress sensitivity. *R* becomes even more stress path sensitive, which is due to the increasing trend of the stiffness $\Delta\sigma_z/\Delta\varepsilon_z$ with increasing stress path κ.

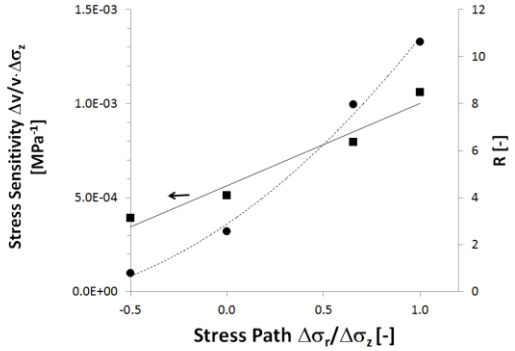

Figure 2: Ultrasonic stress and strain (*R*) sensitivity for the axial P-wave velocity versus stress path parameter $\kappa = \Delta\sigma_r/\Delta\sigma_z$ for a brine saturated field shale core (sample axis ⊥ bedding plane).

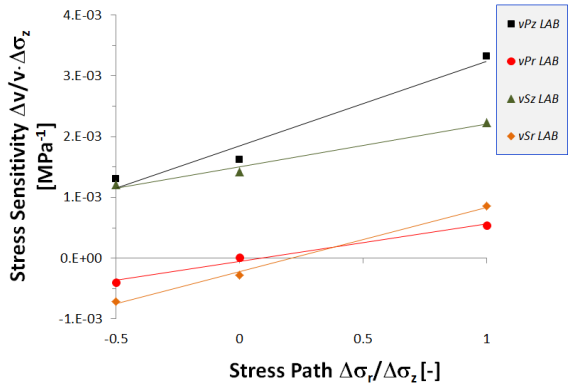

Figure 3: Ultrasonic stress sensitivity for the axial P-wave velocity versus stress path parameter $\kappa = \Delta\sigma_r/\Delta\sigma_z$ for anon-saturated core from a gas shale (sample axis ⊥ bedding plane).

We have observed this behavior in several shales, and it is also seen for other modes of propagation than the axial P-wave. An example is shown in Figure 3, where stress sensitivities of axial and radial P- and S-wave velocities are plotted vs. stress path from a laboratory test with a gas shale field core. Here, no pore pressure was applied, and only three stress paths were probed. The linear trend of the stress path sensitivity is manifested.

Experimental data: Low frequency measurements

A Pierre Shale sample which has been conditioned to prescribed relative humidity (19%) was used for testing in the low frequency apparatus. Simultaneous ultrasonic (P-wave) velocity measurements were done, again along the four different stress paths described above. In order to estimate the low frequency stress sensitivity, one has to perform an anisotropic conversion from the measured Young's modulus and Poisson's ratio into the relevant stiffness for axial P-wave velocity (C_{33}). This conversion utilizes measurements from other samples with different orientations, which in case of non-perfect sample orientation or non-homogeneous core material may introduce significant uncertainty.

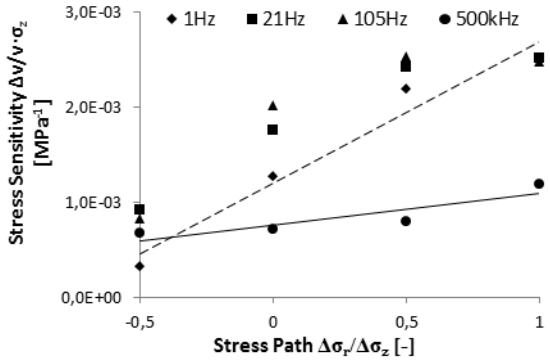

Figure 4: Ultrasonic and seismic stress path sensitivity of Pierre shale. Low-frequency data were obtained by TI symmetry conversion to P-wave velocities from Young's moduli and Poisson's ratios measured for 3 differently oriented samples. Ultrasonic and low frequency data for given orientation were measured within single experiment.

Figure 4 shows the result of the test with Pierre Shale. Again, the same trend in stress path sensitivity as seen above is reproduced with ultrasonic as well as low frequency data. The most striking difference is the much larger (a factor of ~ 3) stress sensitivity observed in the seismic frequency range. Notice that the measured velocity dispersion, i.e. the difference between ultrasonic and seismic frequency P-wave velocity in this case is 5 – 10 %.

Stress Path dependence of Ultrasonic and Seismic Velocities in Shale

Links to *in situ* stress sensitivity

In the previous paragraphs we have seen that stress path sensitivity is observed with ultrasonic as well as seismic frequency measurements. We have also seen that the *in situ* stress path in the overburden depends on geometry and mechanical properties of the reservoir as well as the overburden. Field-tailored geomechanical simulations are required in order to evaluate the sensitivity of seismic velocities with respect to pore pressure changes in a given reservoir.

Here we present a generic approach, obtained by combining experimentally observed stress path dependence of the vertical P-wave velocity with simplified geomechanical modeling, as described above. In order to do this, Eq. (3) has to be rephrased in terms of the stress path coefficients γ_v and γ_h and the *in situ* pore pressure change within the overburden, which is given by the Skempton parameters (Eq. (6)). The result is:

$$\frac{\Delta v}{v} = \gamma_v \left\{ [\frac{A}{3} + B - A_S B_S C] + [\frac{2A}{3} - B - B_S(1 - A_S)C] \frac{\gamma_h}{\gamma_v} \right\} \Delta p_{f,res} \qquad (7)$$

Notice that the ratio between γ_h and γ_v corresponds to the stress path coefficient κ in the laboratory tests.

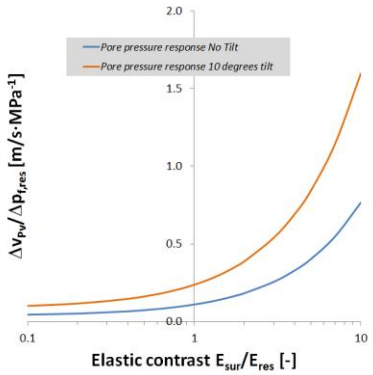

Figure 5: Calculated *in situ* sensitivity of vertical P-wave velocity to reservoir pore pressure depletion versus elastic contrast for a 10° tilted and a non-tilted reservoir, based on the laboratory experiment displayed in Figure 2 and FEM simulations of the *in situ* stress path.

Figure 5 shows the estimated *in situ* stress sensitivity for a fictitious case where the aspect ratio of the depleting zone is 0.10. In the geomechanical model, rocks are assumed isotropic (which is a simplification; Li *et al*., 2014), and we assume that the Poisson's ratio is the same (0.30) within the reservoir and its surroundings. Elastic contrast is accounted for in the ratio between Young's modulus of the surroundings and the reservoir. Ultrasonic laboratory data from a field shale is used to produce the graphs. The figure shows that if the overburden is stiff compared to the reservoir rock, and in particular if it is tilted, the effect on 4D time shifts will be much larger than in the classical case of the Geertsma model (E_{sur}/E_{res}=1). The actual numbers on the axis will depend on the relevant shale: The shale in Figure 5 has relatively low stress sensitivity. Also, if the observation made with Pierre Shale is generally valid, the seismic stress sensitivity could be much larger than that derived from ultrasonics for all elastic contrasts.

Conclusions

Laboratory experiments with field and outcrop shales have been used to demonstrate that the assumption of linear stress sensitivity, leading to predictable stress-path sensitivity, is valid for shales within a stress range relevant for those associated with the overburden above depletion or injection sites. There is indication that the seismic frequency stress sensitivity, linked to the dispersion mechanism, may be larger than ultrasonic stress sensitivity in shale. Geomechanical modeling can translate the laboratory measured stress path sensitivity into expected velocity changes in the field.

Obviously, one has to take care with respect to the representativeness of core material for the scale of the overburden and the reservoir. Nevertheless, the knowledge gained from controlled laboratory experiments should be considered as an important part of the understanding required in order to plan and analyze data from 4D seismic surveys with respect to recovery from hydrocarbon reservoirs or the successfulness of subsurface CO_2 storage.

Acknowledgements

The authors would like to acknowledge financial support from The Research Council of Norway, BP, DONG Energy, Engie, Maersk and Total through the KPN-project "Shale Rock Physics: Improved seismic monitoring for increased recovery" at SINTEF Petroleum Research, and through the ROSE program at NTNU.